SPIRE Spectrometer Pipeline Description

SPIRE-BSS-DOC-002966

Trevor Fulton

Issue 1.0
23 May 2008

SPIRE Spectrometer Pipeline Description

Trevor Fulton

Table of Contents

Chapter 1. Introduction

1.1. Acronyms

Table 1.1. Acronyms

Short Form	Full Name
ADC	Analog to Digital Converter
FFT	Fast Fourier Transform
FT	Fourier Transform
FTS	Fourier Transform Spectrometer
iFTS	Imaging Fourier Transform Spectrometer
ILS	Instrument Line Shape
IPAC	Infrared Processing and Analysis Center
JPL	Jet Propulsion Laboratory
LHS	Left Hand Side
LPF	Low Pass Filter
MPD	Mechanical Path Difference
NHKT	Nominal HouseKeeping Timeline Product
OPD	Optical Path Difference
QCP	Quality Control Pipeline
RC	Resistor-Capacitor
RHS	Right Hand Side
RMS	Root Mean Square
RSRF	Relative Spectral Response Function
SBS	Spectrometer Beam Splitter
SCAL	Spectrometer Calibrator
SDI	Spectrometer Detector Interferogram Product
SDS	Spectrometer Detector Spectrum Product
SDT	Spectrometer Detector Timeline Product
SLW	Spectrometer Long Wavelength Detector Array
SMEC	SPIRE Spectrometer Mechanism
SMECT	Spectrometer Mechanism Timeline Product
SOF	Spectromter Observation Format
SPG	Standard Product Generation
SPIRE	Spectral and Photometric Imaging REceiver
SPP	SPIRE Pointing Product
SSW	Spectrometer Short Wavelength Detector Array
TBD	To Be Determined
TBW	To Be Written
WTMML	Wavelet Transform Modulus Maxima Lines
ZPD	Zero Path Difference

1.2. Scope of Document

This purpose of this document is to present an outline of the processing steps in the SPIRE spectrometer pipeline. The processing modules presented in this document follow those presented in Section 3 of [AD01], which describes the steps that are common to both the SPIRE spectrometer and photometer pipelines.

1.3. Documents

1.3.1. Applicable Documents

AD01   M Griffin, The SPIRE Analogue Signal Chain and Photometer Detector Data Processing Pipeline, SPIRE-UCF-DOC-002890, Issue 4, 20 February 2008.

AD02   T. L. Lim, SPIRE Pipeline Description, SPIRE-RAL-DOC-002437

AD03   SPIRE Observers' Manual, HERSCHEL-HSC-DOC-0789, Version 1.2, 11 September 2007, http://herschel.esac.esa.int/Docs/SPIRE/html/spire_om.html.

AD04   K. J. King, SPIRE Data Product Definition

AD05   Operating Modes for the SPIRE Instrument, SPIRE-RAL-DOC-0000320, Issue 3.3, 24 June 2005.

1.3.2. Reference Documents

RD01   Jean-Paul Baluteau, PFM3b data: some SMEC or FTS performances, Presentation to SDAG 15, 10 July 2006

RD02   Sensitivity of the SPIRE Detectors to Operating Parameters, SPIRE-UCF-DOC-002901, 14 November 2007

RD03   D. A. Naylor and M. K. Tahic, "Apodizing functions for Fourier transform spectroscopy," J. Opt. Soc. Am. A 24, 3644-3648 (2007)

1.4. Document History

Table 1.2. Version and Date

Issue	Date
Draft 0.1	27 March 2007
Draft 0.2	02 May 2007
Draft 0.3 (was Version 1.0)	09 May 2007
Draft 0.4 (was Version 1.1)	27 June 2007
Draft 0.5 (was Version 1.2)	10 July 2007
Draft 0.6 (was Version 1.3)	31 August 2007
Draft 0.7 (was Version 1.4)	26 September 2007
Draft 0.8 (was Version 1.5)	02 October 2007
Draft 0.9 (was Version 1.6)	10 April 2008

Chapter 2. SPIRE Spectrometer Pipeline Overview

2.1. Basic Pipeline Overview

The purpose of the SPIRE spectrometer data processing pipeline is to transform the spectrometer detector samples acquired during a single building block of a single SPIRE spectrometer observation into a set of spectra. In scanning mode, a building block consists of a set of scans of the spectrometer mechanism of the same resolution, with each scan defined as a single movement of the mechanism from one extreme position to the other.

The first steps of the SPIRE spectrometer and photometer pipelines are identical and are described in Section 3 of [AD01]. The SPIRE spectrometer pipeline modules that follow from that common processing pipeline perform five basic operations, which are listed below:

1. **Modify Timelines**

   The processing modules in this group perform time domain operations on the spectrometer detector samples.

2. **Create Interferograms**

   The processing modules in this group merge the timelines of the spectrometer detectors and spectrometer mechanism into interferograms. The spectrometer detector samples are split into different sets, with each set defined by a single scan of the spectrometer mechanism.

3. **Modify Interferograms**

   The processing modules in this group perform operations on the spectrometer detector interferograms. These operations differ from those in the "Modify Timelines" group in that they are designed to act on spatial domain data rather than time domain data.

4. **Transform Interferograms**

   The processing modules in this group transform the interferograms into a set of spectra.

5. **Modify Spectra**

   The processing modules in this group perform operations on the spectrometer detector spectra.

The manner in which the basic operations relate to one another is shown in Figure 2.1.

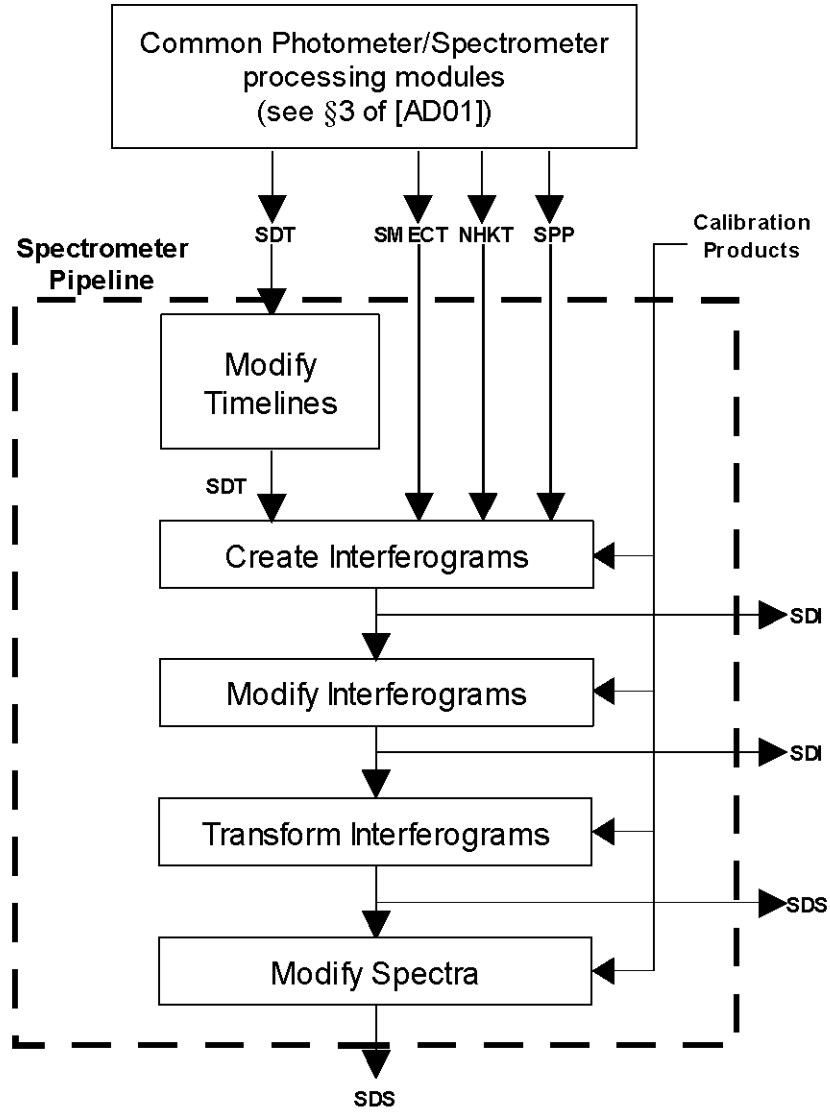**Figure 2.1. Basic Processing Operations of the SPIRE Spectrometer Pipeline**

2.2. Detailed Pipeline Overview

The individual processing modules in the SPIRE spectrometer pipeline and their connection with one another are shown in Figure 2.2. Descriptions of the current implementation of these processing modules are presented in Chapter 3.
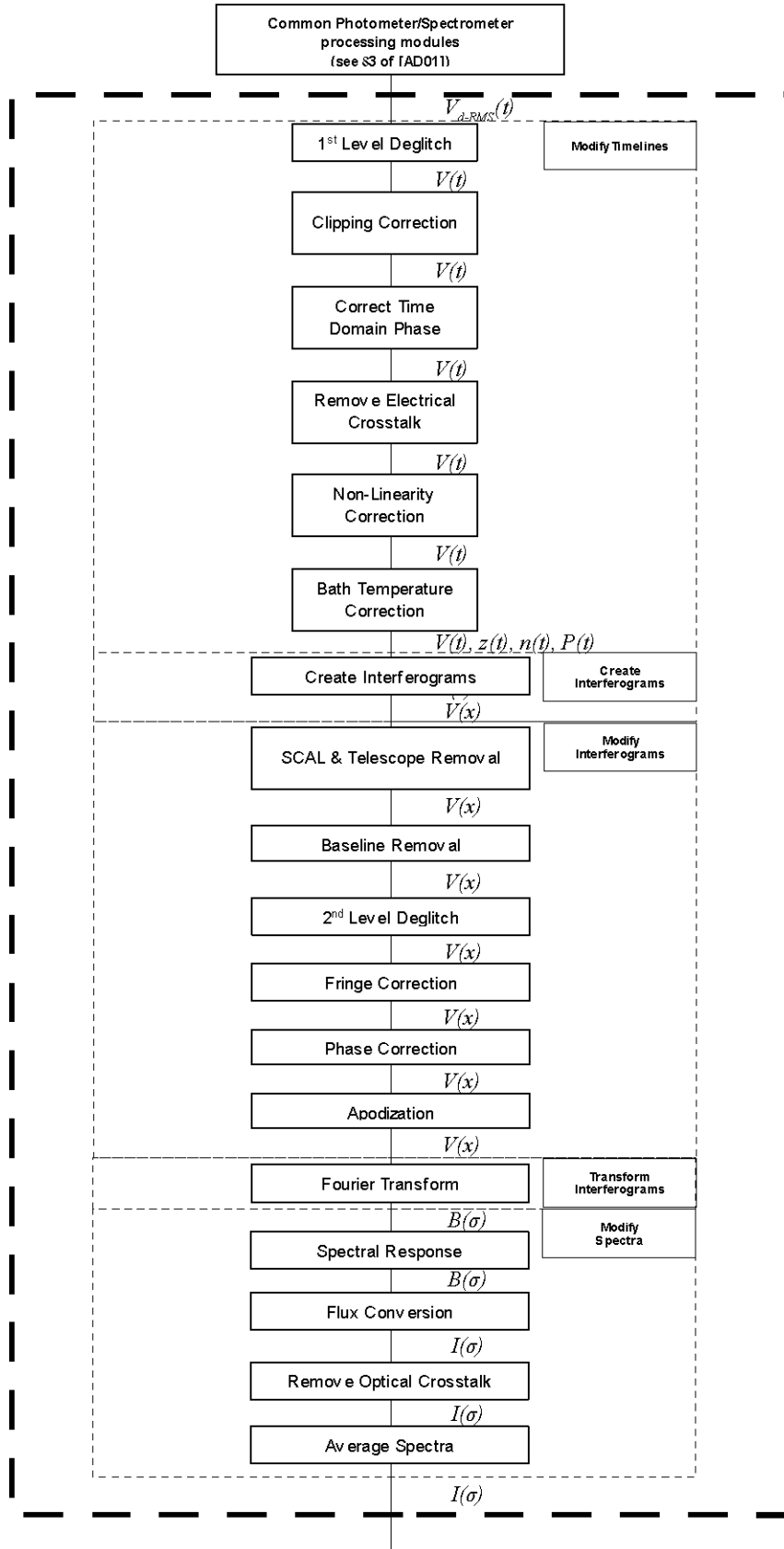
Figure 2.2. Detailed functionality of the SPIRE Spectrometer pipeline.

Chapter 3. Spectrometer Pipeline

3.1. Modify Timelines

As listed in Figure 2.2, the first steps of both the spectrometer and photometer pipelines are identical and are described in Section 3 of [AD01]. After application of the processing steps described in section 3 of [AD01], the raw samples for each spectrometer detector, i, will have been converted into RMS voltage and current timelines as denoted by: $V_{d\text{-RMS-}i}(t)$ and $I_{b\text{-RMS-}i}(t)$, respectively. These quantities are contained in the Level 0.5 Spectrometer Detector Timeline Product.

The timeline modification block is shown in Figure 3.1.
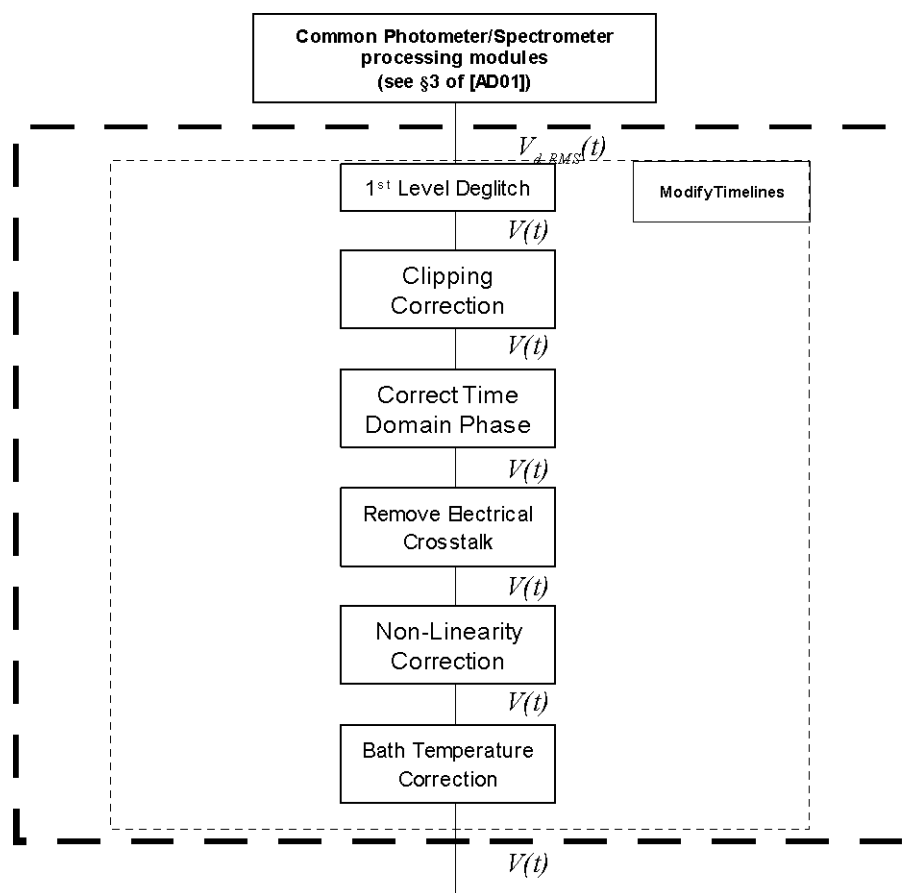
Figure 3.1. Timeline modification block of the SPIRE Spectrometer pipeline

The processimg modules described in the following section are applied to the timelines for each spectrometer detector.

3.1.1. First Level Deglitching

Glitches due to cosmic ray hits or other impulse-like events in the detectors will be removed using an algorithm based on a wavelet-based local regularity analysis (see Section A.1). This process is composed of two steps: the first step detects glitch signatures over the measured signal; the second step locally reconstructs a signal free of such glitch signatures.

1. **Glitch Identification.** Glitches are detected in the input SDT product by wavelet analysis as-

suming that the glitch signature is similar to the signature of a Dirac delta function

2. **Glitch Removal.** Each glitch flagged by the preceding step is contains localized wavelet coefficients specific to the glitch. These coefficients are removed and a local, inverse wavelet transform is performed to create an SDT product that is free of glitches.

The output of this module is the deglitched voltage timeline, $V_{1-i}(t)$ for detector i.

3.1.2. Removal of Electrical Crosstalk

After de-glitching, let the timeline for bolometer i be denoted as $V_{1-i}(t)$. This timeline might contain contributions that depend on the signals from other detectors due to either electrical or optical crosstalk. Electrical crosstalk arises after the detector and is due to capacitative or inductive coupling between the detector readout channels. Optical crosstalk occurs before the detector and is due to diffraction or aberrations in the optical system causing some of the power from an astronomical source to fall on inappropriate detectors.

Electrical crosstalk can be removed if the coupling between the detectors is known, and it is appropriate to do it at this stage.

Here it is assumed that:

1. electrical crosstalk is linear, so that the effects can be characterised by a crosstalk matrix, C_{elec}, with constant elements;

2. electrical crosstalk from one detector to another involves negligible diminution of the signal in the primary detector;

3. there is no crosstalk between different arrays.

For a particular time-step, the vector of electrical crosstalk-corrected signals is given by $V_2 = C_{elec} V_1$. As an illustration, with three detectors, the matrix equation would be

Equation 3.1.

$$\begin{bmatrix} V_{2-1} \\ V_{2-2} \\ V_{2-3} \end{bmatrix} = \begin{bmatrix} 1 & e_{21} & e_{31} \\ e_{12} & 1 & e_{32} \\ e_{13} & e_{23} & 1 \end{bmatrix} \begin{bmatrix} V_{1-1} \\ V_{1-2} \\ V_{1-3} \end{bmatrix}.$$

The electrical crosstalk matrix may be implemented as a calibration file. Determination of the elements of the electrical crosstalk matrix is a difficult problem. One possibility is to use the occasional ionizing radiation hits that the bolometers will experience. Ideally, a single event in a bolometer produces a spike only in its own output; crosstalk results in this being accompanied by lower-level responses from other detectors.

3.1.3. Clipping Correction

The purpose of this processing step is to correct for clipping of the measured signals due to the limited range of the detector ADCs.

Clipped signals in the SDT are problematic as they represent missed samples in the timeline. If left uncorrected, missed or erroneous samples can lead to further complications in particular when the timelines are converted into interferograms (Section 3.2.1).

Missed or erroneous samples can be corrected in a given SDT timeline as long as the number of consecutive missed samples SDT does not result in a violation of the Nyquist criteria. For sampled

signals the Nyquist frequency defines the maximum independent frequency that is sampled. Using the nominal SPIRE spectrometer scanning parameters, the Nyquist frequency exceeds the maximum SLW frequency by a factor of 6 and exceeds the maximum SSW frequency by a factor of 4. As such, the sampled signals can be completely reconstructed even in the abscence of five consecutive samples for SLW and three consecutive samples for the SSW detectors.

The process by which clipped timelines are corrected is described below.

1. **Identify the clipped samples in the SDT timelines.** Let $V_{2-i}(t_k)$ denote those samples that have been flagged as being clipped, and let $V_{2-i}(t_j)$ represent all other samples, each of which for a given spectrometer detector, i.

2. **Check the number of consecutive clipped samples in SDT timelines.** If the number of consecutive clipped samples exceeds five for the SLW detectors or three for the SSW detectors then discontinue the correction and set the appropriate flag for the Quality Control Pipeline (QCP).

3. **Subsample the SDT timeline.** The SDT is subsampled by an integer multiple, M, so that the clipped signals are omitted.

Equation 3.2.

$$V'_{2-i}(t) = V_{2-i}(t:0:N_{Samples}:M)$$

4. **Interpolate the subsampled SDT timeline.** Interpolation of the subsampled SDT is performed by first computing its spectrum. If the Nyquist criteria is satisfied then the in-band spectrum of the subsampled timeline will be identical to that of the original timeline. The subsampled spectrum is then padded with zeroes to the original Nyquist frequency. Finally, the inverse Fourier transform is applied to the padded spectrum in order to recover the signal at the orignal sampling rate.

Equation 3.3.

$$B'_{2-i}(f) = FT\left[V'_{2-i}(t)\right]$$

Equation 3.4.

$$B''_{2-i}(f) = B'_{2-i}(f)\big|_0^{f'_{MAX}}, 0\big|^{f'_{MAX} < f \leq f_{MAX}}$$

Equation 3.5.

$$V''_{2-i}(t) = FT^{-1}\left[B''_{2-i}(f)\right]$$

5. **Replace the SDT timeline.** Replace only those samples, t_k that had been identified as clipped in the original detector timeline, $V_{2-i}(t)$. Samples that were not identifies as being clipped, $V_{2-i}(t_j)$ are simply propagated to the resultant timeline, $V_{3-i}(t)$.

Equation 3.6.

$$V_{3-i}(t_j) = V_{2-i}(t_j)$$

Equation 3.7.

$$V_{3-i}(t_k) = V''_{2-i}(t_k)$$

Note

Currently, any SDT that contains clipped signals is flagged for the QCP for further inspection. SPIRE spectrometer observations flagged in this manner will be investigated by the Quality Control engineer to see if any valid astronomical products can be derived.

3.1.4. Time Domain Phase Correction

As mentioned in Section 3.7 of AD01, the SPIRE spectrometer detector chain contains a 6-pole Bessel low pass filter (LPF) as well as an additional RC LPF the transfer function of which is shown below.

Equation 3.8.

$$H_{LPF-S}(\omega_S) = \left[\frac{2.87}{1 + 7.85 \times 10^{-3}(j\omega_S) + 16.03 \times 100^{-6}(j\omega_S)^2}\right] \times \left[\frac{1}{1 + 3.23 \times 10^{-3}(j\omega_S) + 400 \times 100^{-6}(j\omega_S)^2}\right] \times$$
$$\left[\frac{1}{1 + 6.26 \times 10^{-3}(j\omega_S) + 14.65 \times 100^{-6}(j\omega_S)^2}\right] \times \left[\frac{1}{1 + 1 \times 10^{-4}(j\omega_S)}\right]$$

In addition to the electronic LPF, the thermal behaviour of the SPIRE bolometers can be modeled as a simple RC LPF with a detector-specific time constant, τ.

Equation 3.9.

$$H_{LPF-Thermal}(\omega) = \left[\frac{\omega_{Thermal}}{(j\omega) + \omega_{Thermal}}\right]$$

These two effects may be combined into a single detector transfer function, given by the following:

Equation 3.10.

$$H_{TOTAL}(\omega_S) = \left[\frac{2.87}{1 + 7.85 \times 10^{-3}(j\omega_S) + 16.03 \times 100^{-6}(j\omega_S)^2}\right] \times \left[\frac{1}{1 + 3.23 \times 10^{-3}(j\omega_S) + 400 \times 100^{-6}(j\omega_S)^2}\right] \times$$
$$\left[\frac{1}{1 + 6.26 \times 10^{-3}(j\omega_S) + 14.65 \times 100^{-6}(j\omega_S)^2}\right] \times \left[\frac{1}{1 + 1 \times 10^{-4}(j\omega_S)}\right] \times \left[\frac{\omega_{Thermal}}{(j\omega) + \omega_{Thermal}}\right]$$

As noted in Section 3.7 of AD01, the LPFs will affect the magnitude of the signal recorded by the SPIRE detectors. In addition, the LPFs will induce a phase shift to the recorded signal. The overall phase imparted by the combined effects of the LPF and the thermal response is then given by:

Equation 3.11.

$$\phi_{TOTAL}(\omega_S) = \tan^{-1}\left[\frac{\Im\left(H_{TOTAL}(\omega_S)\right)}{\Re\left(H_{TOTAL}(\omega_S)\right)}\right]$$

The phase shift from the combination of the read-out electronics and the thermal response of the detectors manifests itself, to first order, as a delay in time of the recorded signal. This effect is particularly problematic for the SPIRE spectrometer in scanning mode (SOF1 and SOF2), where the delay induced by the electronic and thermal phase can lead to errors in the interpolation of the detector signals(see Section 3.2.1).

The measured detector timelines are corrected by first characterizing the phase shift (as above) then by deriving a time domain phase correction function (PCF)

Equation 3.12.

$$PCF_t(t) = FT^{-1}\left[e^{-\phi_{TOTAL}(\omega_S)}\right]$$

4 Convolution of the measured detector timelines with the derived time domain phase correction function results in a corrected timeline.

Equation 3.13.

$$V_{4-i}(t) = V_{3-i}(t) \otimes PCF_{t-i}(t)$$

3.1.5. Detector Non-Linearity Correction

Even though bolometric detectors are commonly fabricated with highly linear response characteristics, the detectors of the SPIRE spectrometer will be subject to a wide dynamic range which makes a non-linear response likely. A dedicated non-linearity correction is designed to account for changes in the response of the detectors to strong signals. The form of this correction will be a function that is dependent on the amplitude of the signal itself as in Equation 3.14:

Equation 3.14.

$$V_{5-i}(t) = \int_{V_0}^{V_{4-i}} \frac{f(V)}{f(V_r)}\,dV$$

where f(V), the real detector responsivity, V_r is a reference voltage, and V_0 is a fixed bolometer voltage. The normalized value of f(V) is derived as in (Equation 3.15):

Equation 3.15.

$$\frac{f(V)}{f(V_r)} = K_1 + \frac{K_2}{V - K_3}$$

A calibration table will contain the values for V_0, K_1, K_2, and K_3 for each detector. Distinct calibration tables will be used for each detector bias configuration and for each value of V_0. and V_r. Initially, the quantities in these calibration tables will be based on model predictions.

3.1.6. Removal of correlated noise due to bath temperature fluctuations

To first order, bath temperature fluctuations will influence all detectors in an array coherently -- the temperature and corresponding output voltages will go up and down in synchronism. The bath temperature, T_o, may fluctuate due to temperature drifts within the instrument, and a set of timelines, $V_{th-i}(t)$, must be generated to correct for this. The most important effect of bath temperature variations for the level of fluctuations expected in SPIRE, will be the direct response of the detector output voltage. Fluctuations in T_o are expected to be much faster than a single, high-resolution scans of the spectrometer mechanism, so that this correction will be needed for such observations.

A correction timeline for each detector, $V_{th-i}(t)$, will be generated by way of a suitable algorithm using thermometry data (to be based on evaluation carried out on data by IPAC/JPL). This timeline is then subtracted from that detector's signal timeline, $V_{5-i}(t)$. In order to avoid introducing additional noise to the corrected detector timeline, the $V_{th-i}(t)$ timeline will need to be significantly less noisy than the bolometer signals. It will therefore need to be averaged over a period of time such that it becomes a negligible fraction of the detector noise. This will require a suitable averaging period (JPL/IPAC assessment of the data indicates that a period on the order of a second or a few seconds is suitable). Thermal fluctuations on timescales shorter than this will not be tracked.

The output of this module is a set of spectrometer detector voltage timelines corrected for low-frequency thermal drifts: $V_{5-i}(t)$ for detector i.

3.2. Create Interferograms

The pipeline modules listed to this point describe the operations that will be performed on the Level 0.5 timelines of the spectrometer detectors. At this point, it should also be mentioned that three additional Level 0.5 timelines will also be required for the next step in the spectrometer processing pipeline. These additional timelines are the Spectrometer Mechanism timeline, the Nominal Housekeeping timeline, and the SPIRE Pointing timeline. These three timelines, as well as the modified Spectrometer Detector timeline serve as the inputs to the next step in the spectrometer processing pipeline.

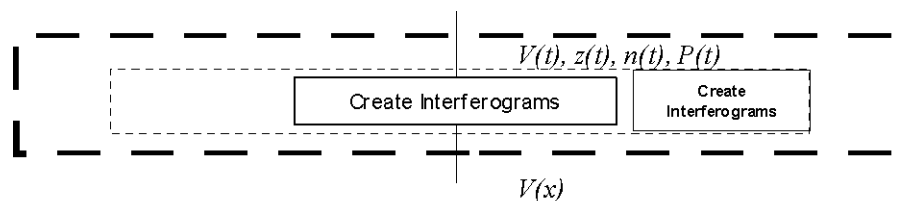The interferogram creation block is shown in Figure 3.2.

Figure 3.2. Interferogram creation block of the SPIRE Spectrometer pipeline

3.2.1. Interferogram Creation

A single building block of a SPIRE spectrometer observation in scanning mode consists of a series of scans of the spectrometer mechanism while the instrument is pointed at a given target. The sampling of the SPIRE spectrometer detectors and the spectrometer mechanism is decoupled; the two subsystems are sampled at different rates and at different times. In order to derive the source spectrum from the measured data, the spectrometer detector samples must be linked with the position of the SMEC in the form of interferograms. Additionally, the SMEC positions onto which the spectrometer detector signal samples are to be interpolated should be regularly-spaced in terms of optical path difference (OPD). The purpose of this step is to ensure proper transformation of the interferogram with the Discrete Fourier Transform.

The process by which interferograms are created involves two steps, each of which is described below.

1. **Interpolation of the SMEC timeline.** This step converts the spectrometer mechanism timeline from one that is non-uniform in position to one that is uniform in position.

   a. **Establish a common OPD position vector.** This step creates a common vector of OPD positions that will be the basis of the interferograms for all of the spectrometer detectors and for all of the scans in the observation. This common position vector will contain samples that are uniformly-spaced in terms of OPD position as well as a sample at the position of zero-path-difference (ZPD).

   The step size of the common OPD vector is chosen is such a way as to match the sampling rate of the spectrometer detector signal samples. For an SDT sampling rate s [Hz] and a SMEC scanning speed v_{SMEC} [cm/s MPD], the position step size, δMPD in units of cm; is given by:

   Equation 3.16.

   $\delta MPD = v_{SMEC} / s$

   This step is then converted such that it is in terms of OPD by the following relation

   Equation 3.17.

   $\delta OPD = INT[4\delta MPD]$

   where INT[] denotes that the step size is rounded to the nearest integer in units of μm OPD and the factor of four is the nominal conversion between MPD and OPD for a Mach-Zehnder FTS. Using the nominal SPIRE spectrometer settings -- s=80Hz, v_{SMEC}=0.05cm/s -- this results in an OPD step size of 25 μm.

   b. **Map the common OPD position vector to a SMEC position vector for each spectrometer detector.** This step maps, for each spectrometer detector, the common OPD positions established in the preceding positions in units of mechanical path difference. This step involves: a scaling factor, f, that takes into account the step size for a Mach-Zehnder FTS; and a shifting factor, ZPD, which establishes the position of zero optical path difference. Since these quantities are unique to each spectrometer detector, i, this mapping is performed on a detector-by-detector basis and is shown in ???.

   Equation 3.18.

   $$MPD_i = \frac{OPD}{f_i} + ZPD_i$$

   c. **Parse the measured SMEC timeline into discrete scans.** This step splits the full SMEC timeline ($z(t_{SMEC})$) from the input SMECT product into a series of discrete timelines, $z_n(t_{SMEC})$. Each of the discrete timelines, $z_n(t_{SMEC})$, represents one spectrometer scan. The delineation of the SMEC timeline is accomplished by comparing consecutive SMEC position samples and finding those samples where the motion of mirror mechanism changed direction.

   d. **Interpolate the measured SMEC timelines onto the mapped SMEC timelines.** The next step is to determine, on a detector-by-detector and scan-by-scan basis, the times when the spectrometer mechanism reached the mapped SMEC positions. Since, for each detector, there is a 1:1 relationship between the mapped SMEC positions and the regularly-spaced OPD positions, this step effectively determines the times when the SMEC reached the regularly-spaced OPD positions for each detector.

   Equation 3.19.

$$z_n\left(t_{SMEC}\right) \rightarrow MPD_{n-i}\left(t_{MPD-i}\right)$$

2. **Merge the spectrometer detector and the mapped SMEC timelines.** This step combines the signal samples from the signal timeline of a given spectrometer detector ($V_{5-i}(t_i)$) with the mapped SMEC timelines.

   a. **Interpolation of the spectrometer detector timelines.** The spectrometer detector signal samples are mapped onto the times corresponding to the regular MPD (t_{MPD-i}) positions by way of interpolation. Since there is a 1:1 relationship between these time samples, t_{MPD-i}, and the regular MPD positions, MPD_i, this interpolation effectively maps, for each detector, the signal samples to the regularly-spaced MPD positions. Moreover, since there is a 1:1 relationship between the regular MPD positions for each detector and the common OPD positions, this step accomplishes the mapping of the signal samples for each detector to the common OPD positions, which is the resultant interferogram that is desired.

   Equation 3.20.

   $$V_{5-i}\left(t_i\right) \rightarrow V_{6-i}\left(t_{MPD-i}\right) \rightarrow V_{6-i}\left(t_{OPD}\right) \rightarrow V_{6-i}\left(OPD\right) \equiv V_{6-i}\left(x\right)$$

The process outlined above is repeated for all spectrometer detectors for each scan of the observation building block. The resultant interferograms are then combined into a single Spectrometer Detector Interferogram (SDI) product. In addition, the mean value of the pointing, P(t), as derived from the input SPIRE Pointing product (SPP) for the observation building block is assigned to the output SDI product.

3.3. Modify Interferograms

The pipeline modules described in this section perform operations on the spectrometer detector interferograms created in the previous step.

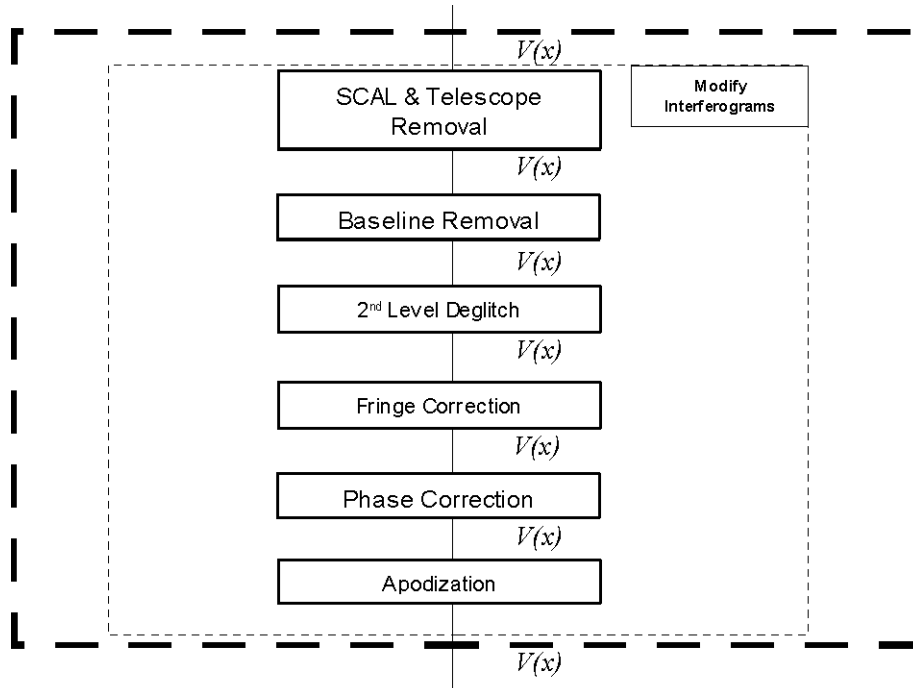The timeline modification block is shown in Figure 3.3.

Figure 3.3. Interferogram modification block of the SPIRE Spectrometer pipeline

3.3.1. SCAL and Telescope Correction

The equation for the total intensity of the radiation incident upon the spectrometer detectors shows that, in addition to radiation from the astronomical source, the detectors record a modulated signal from the Herschel Telescope and from each of the components of the spectrometer calibrator (SCAL). This processing step removes these components from the measured interferogram.

Equation 3.21.

$$V_{6-i}(x) = \left(V_{6-Source-i}(x) + V_{6-Telescope-i}(x) + V_{6-SCAL-i}(x) + V_{6-SCAL2-i}(x) + V_{6-SCAL4-i}(x) \right)$$

The method employed in the simple pipeline to correct for the Herschel Telescope and the SCAL components is to subtract from the measured interferogram ($V_{6-i}(x)$) a interferogram derived from a calibration observation wherein the Telescope is pointed at blank sky ($V_{6-ref-i}(x)$). This calibration observation will also have both SCAL2 and SCAL4 set to the same temperatures as was the case for the on-source observation.

Equation 3.22.

$$V_{6-ref-i}(x) = \left(V_{6-Telescope-ref-i}(x) + V_{6-SCAL-ref-i}(x) + V_{6-SCAL2-ref-i}(x) + V_{6-SCAL4-ref-i}(x) \right)$$

Equation 3.23.

$$V_{7-i}(x) = V_{6-i}(x) - V_{6-ref-i}(x)$$

In the model-based pipeline, removal of the Telescope and SCAL contributions is performed by subtraction of a model their contributions derived from the measured temperatures of each element and the measured transmission through the spectrometer for each emitting element. This method has the advantage of not requiring a blank-sky calibration observation though the precision of such a method cannot be evaluated until flight conditions are observed.

The result of the Telescope and SCAL correction step will be a set of interferograms for each spectrometer detector ($V_{7-i}(x)$); these interferograms are stored in an SDI product. The principal component of the resultant interferograms is radiation from the astronomical source.

3.3.2. Interferogram Baseline Correction

According to the equations presented in Section A.2, the overall intensity incident on the SPIRE spectromter detectors can be separated into two components: a component that is constant as a function of OPD; and a component that is modulated as a function of OPD. As the offset term does not contain any spectral information, it may be removed without affecting the source spectrum.

On a detector-by-detector and scan-by-scan basis, the baseline correction algorithm evaluates and removes the offset portion of the derived interferogram ($V_{7-i}(x)$). The preferred manner to evaluate the offset is to fit a fourth-order polynomial to the measured interferogram.

Equation 3.24.

$$V_{Baseline-i}(x) = a_i + b_i x + c_i x^2 + d_i x^3 + e_i x^4$$

Once evaluated, the fitted function is removed from the measured interferogram by subtraction.

Equation 3.25.

$$V_{8-i}(x) = V_{7-i}(x) - V_{Baseline-i}(x)$$

3.3.3. Second Level Deglitching

Localized artifacts in the interferograms, glitches, pose a serious problem for Fourier Transform Spectrometer observations. As such, a glitch that affects as few as one interferogram sample can adversely affect each and every spectral component. Glitches in an interferogram must therefore be identified and removed prior to transformation in order to avoid unwanted spectral artifacts.

Glitches are identified for each spectrometer detector by comparing, on a OPD-position-by-OPD-position basis, the samples from one scan to those from all other scans in the same observation. The samples that deviate more than a prescribed amount from the median are flagged as glitches.

The samples that are identified as glitches are then replaced. For a glitch at a given position for a given spectrometer detector, the value of the replacement sample is determined by the average of the non-glitch samples from the other observed interferograms at that position.

Equation 3.26.

$$V_{j-8-i}(x_k) = \frac{1}{N_{scans}-1} \sum_{n=i, n \neq j}^{N_{scans}} V_{n-8-i}(x_k)$$

Note

The two steps of the interferogram deglitching module rely on a statistical analysis of the measured interferograms. As such, a minimum number of six interferograms per building block will be required so that these statistics will be meaningful.

3.3.4. Channel Fringe Correction

The effect of channel fringes on spectrometer data is similar to that of glitches (Section 3.3.3). If left uncorrected the channel fringes will contaminate the measured spectrum. Currently, three different algorithms are being evaluated as possible methods to correct for channel fringes. These are:

Two other methods of fringe correction are under consideration. These methods are:

1. **Apodization.** The application of an apodization function (Section 3.3.6) is currently the baseline method for fringe correction. While apodization is effective at removing the spectral artifacts due to the channel fringes, its application results in a reduction of the observed spectral resolution. Given that the fringe features appear at the extreme high-resolution OPD end for the SLW array and at the extreme medium-resolution end for the SSW array, however, the reduced resolution is not expected to be significant for those observing modes.

   With apodization (Section 3.3.6) chosen as the preferred method of fringe correction, there is no need for a separate fringe correction processing step.

2. **Interferogram Truncation.** This method of channel fringe removal involves truncating the interferogram prior to the channel fringe region. The drawback to this method is similar to that for apodization; reduced spectral resolution.

3. **Iterative Subtraction.** This method of channel fringe correction is performed by removing successive copies of the interferogram in the region near ZPD from the wing portion of the interferogram.

3.3.5. Phase Correction

The symmetry of a Fourier Transform spectrometer theoretically implies that interferograms recorded by the spectrometer will exhibit even symmetry. Since the spectrum of an evenly symmetric interferogram contains only real components, it is therefore expected that the phase should be zero for all spectral components.

The presence of dispersive elements and the possibility that the position of zero path difference not being sampled can, however, result in a interferogram whose *signal* samples are not symmetric about ZPD. The spectrum calculated from this sort of asymmetric interferogram will contain both real and imaginary components and therefore a non-zero phase.

The phase correction module is separated into two components: the first step identifies whether any phase is present in the measured interferogram; the second step removes this phase.

1. **Phase Identification.** The first step of the phase correction process is to identify whether the measured interferograms contain any non-zero phase. In order to make this determination, the spectrum of the double-sided (see Section A.3.1) portion is computed for each interferogram (Equation 3.27)

Equation 3.27.

$$B_{10-i-DS}(\sigma) = FT\left[V_{10-i}\left(x\Big|_{-L}^{L}\right)\right] = \int_{-L}^{L} V_{10-i}(x) e^{-i2\pi\sigma x} dx$$

The phase of the computed spectrum may be evaluated for each spectral component or wavenumber as in Equation 3.28.

Equation 3.28.

$$\phi_{i-DS}(\sigma) = \arctan\left(\frac{\Im(B_{10-i-DS}(\sigma))}{\Re(B_{10-i-DS}(\sigma))}\right)$$

2. **Phase Removal.** The phase in the measured interferograms having been identified, the next step in the process is phase removal. A fourth-order polynomial fit to the measured in-band phase (see Equation 3.29)) rather than the measured phase itself is used in this process. The basis for using the fitted phase rather than the calculated phase is that, by doing so, the noise associated with the imaginary portion of the computed spectrum remains in the imaginary domain. If the phase is stable and the noise is due primarily to random sources, the usage of a fitting function can lead to an increase in the resultant signal-to-noise ratio by a factor of $\sqrt{2}$.

Equation 3.29.

$$\phi_{fit-i}(\sigma) = a_i + b_i\sigma + c_i\sigma^2 + d_i\sigma^3 + e_i\sigma^4 \Big|_{\sigma_{LOW}}^{\sigma_{HIGH}}$$

A phase correction function (PCF) is then derived from the fitted phase for each interferogram as in Equation 3.30).

Equation 3.30.

$$PCF_i(\sigma) = e^{-i\phi_{fit-i}(\sigma)}$$

The derived PCFs are then applied to spectra computed from each of the interferograms in the input SDI product by way of multiplication (Equation 3.31).

Equation 3.31.

$$B_{11-i}(\sigma) = B_{10-i}(\sigma) \times PCF_i(\sigma)$$
$$= B_{10-i}(\sigma) \times e^{-i\phi_{fit-i}(\sigma)}$$

If the observing mode is low- or medium-resolution, the above represents the final step in the phase correction process. High-resolution observations require an extra step. Phase correction of high-resolution interferograms, proceeds in the interferogram (spatial) domain wherein a convolution of the measured interferogram and the the inverse FT of the PCF is performed (see Equation 3.32).

Equation 3.32.

$$V_{11-i}(x) = V_{10-i}(x) \otimes FT^{-1}\left[PCF_i(\sigma)\right]$$
$$= V_{10-i}(x) \otimes FT^{-1}\left[e^{-i\phi_{fit-i}(\sigma)}\right]$$
$$= V_{10-i}(x) \times \sum_{x=-l}^{l}\left(FT^{-1}\left[e^{-i\phi_{fit-i}(\sigma)}\right]\right)(x)$$

3.3.6. Apodization

The natural instrument line shape (ILS) for a Fourier Transform spectrometer is a cardinal sine, or Sinc function. If the source signal contains features at or near the resolution of the spectrometer, the ILS can introduce secondary maxima in the spectra. The apodization functions available within this module may be used to reduce these secondary maxima at the cost of reducing the resolution of the resultant spectrum. The apodization module in the SPIRE spectrometer data processing pipeline offers a number of apodizing functions that to allow for an optimal trade-off between reduction in the secondary maxima and reduced resolution [RD03].

Apodization is performed by multiplying the input interferograms ($V_{n-11-i}(x)$), on a detector-by-detector and on a scan-by-scan basis with a tapering or apodizing function.

Equation 3.33.

$$V_{12-i}(x) = V_{11-i}(x) \times Apod_i(x)$$

3.4. Transform Interferograms

At this point in the spectrometer pipeline, the operations that are best performed in the interferogram domain have been implemented. From this point on, further processing can take place in the spectral

domain. As such, this presents the opportunity to transform the interferograms for each detector, $V_{n-m-i}(x)$, to the spectral domain. The section describes the process by which the interferograms are traanformed to spectra.

The interferogram transformation block is shown in Figure 3.4.
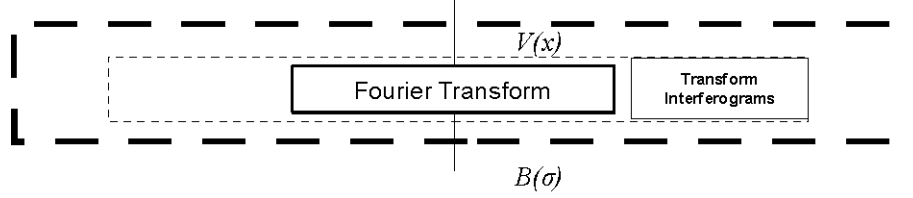

Figure 3.4. Interferogram transformation block of the SPIRE Spectrometer pipeline

3.4.1. Fourier Transform

The purpose of the Fourier Transform module is to transform the set of interferograms from a SPIRE spectrometer observation into a set of spectra. This processing module is capable of transforming both double-sided and single-sided interferograms (see Appendix A for the definition of double-sided and single-sided interferograms).

Double-sided Transform. For the double-sided transform, each interferogram in the SDI is examined and only the double-sided portion of the interferogram is used to compute the resultant spectrum. The resultant spectra will contain both real and imaginary components.

Equation 3.34.

$$B_{12-i}(\sigma) = FT\left[V_{12-i}(x)\Big|_{-L}^{L}\right] = \int_{-L}^{L} V_{12-i}(x)e^{-i2\pi\sigma x}\,dx$$

In this case, the discrete fourier transform that is used to compute the spectral components takes the form shown in Equation 3.35.

Equation 3.35.

$$B(\sigma) = FT\left[I(x)\Big|_{-L}^{L}\right] = \sum_{-L}^{L} I(x)e^{-i\frac{2\pi\sigma x}{N}}$$

Single-sided Transform. In the case of the single-sided transform, only those interferogram samples to one side of the position of zero path difference are considered. The spectra that result from the single-sided transform therefore contain only real components.

Equation 3.36.

$$B_{12-i}(\sigma) = FT\left[V_{12-i}(x)\Big|_{0}^{L}\right] = \int_{0}^{L} V_{12-i}(x)e^{-i2\pi\sigma x}\,dx$$

The discrete fourier transform that is used to compute the spectral components for single-sided interferograms takes the form shown in Equation 3.37.

Equation 3.37.

$$B_{12-i}(k) = \sum_{n=0}^{N-1} V_{12-i}(n) \cos \frac{2\pi k n}{N}$$

Wavenumber Grid. For both the single-sided and double-sided transforms the wavenumber grid onto which the spectrum is registered is calculated based on the interferogram sampling rate (ΔOPD) and on the maximum OPD displacement from the position of ZPD, L.

The Nyquist frequency ($\sigma_{Nyquist}$), the maximum independent frequency in the output spectrum, is given by:

Equation 3.38.

$$\sigma_{Nyquist} = \frac{1}{2\Delta OPD}$$

The spacing between independent spectral samples (Δσ) is given by:

Equation 3.39.

$$\Delta\sigma = \frac{1}{2L}$$

The spacing between spectral samples can be modified by padding the interferogram with zeroes. This procedure does not add any information to the spectrum but allows for an easier comparison between observations. In this case, a zero-padded interferogram ($V_{12\text{-}ZP\text{-}i}$) is given by:

Equation 3.40.

$$V_{12-ZP-i}(x) = V_{12-i}(x)\Big|_0^L, 0\Big|^{L < x \le L_{ZP}}$$

The corresponding spectral sampling interval is given by:

Equation 3.41.

$$\Delta\sigma_{ZP} = \frac{1}{2L_{ZP}}$$

and the resultant spectrum of the zero-padded interferogram is given by:

Equation 3.42.

$$B_{12-ZP-i}(k) = \sum_{n=0}^{N_{ZP}-1} V_{12-ZP-i}(n) e^{-i\frac{2\pi k n}{N_{ZP}}}$$

The scan lengths and resultant spectral sampling intervals for the three distinct spectral resolutions from Section 6.6 of [AD03] are given in Table 3.1.

Table 3.1. Interferogram Padding

Spectral Resolution [AD03]	Sampling Interval (OPD) [μm]	Nyquist Wavenumber [cm^{-1}]	Padded Scan Length (OPD) [cm]	Spectral Sampling Interval [cm^{-1}]
Low	25	200	2.0	0.25
Medium	25	200	10.0	0.05
High	25	200	50.0	0.01

This processing step will create a Level-1 Spectrometer Detector Spectrum (SDS) product that will be available to observers.

3.5. Modify Spectra

The pipeline modules that follow in this section describe the operations that will be performed on the spectrometer detector spectra that were created in the preceding step. The end result of these spectral modifying processing steps will be a Level 1 Spectrometer Detector Spectrum product.

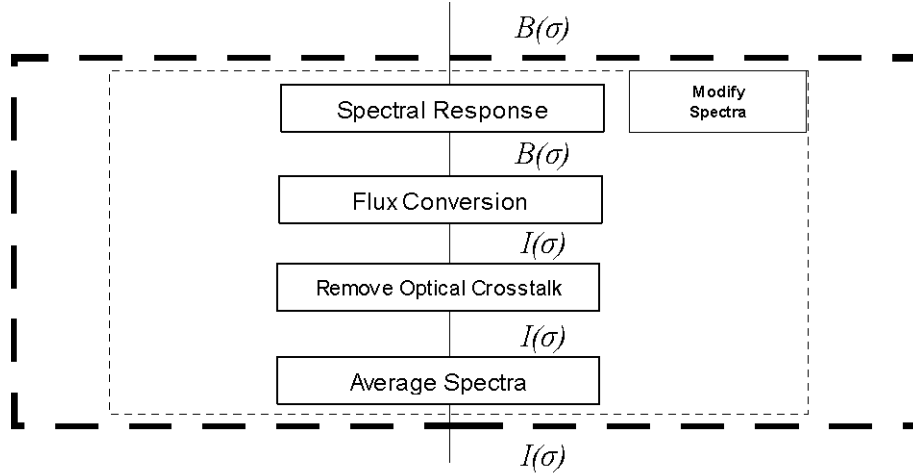The spectral modification creation block is shown in Figure 3.5.

Figure 3.5. Spectral modification block of the SPIRE Spectrometer pipeline

3.5.1. Spectral Response Correction

This module will remove from each measured spectrum for each detector in the input SDS product the relative spectral response function (RSRF) for that particular detector. The correction that is to be applied is given in Equation 3.43.

Equation 3.43.

$$B_{14-i}(\sigma) = \frac{B_{13-i}(\sigma)}{RSRF_i(\sigma)}$$

The RSRF curves for each detector ($RSRF_i(\sigma)$) represent the relative transmission of the SPIRE instrument from the Telescope port to a detector, i. The procedure by which these curves will be derived is given in [RD01].

3.5.2. Flux Conversion

The flux conversion module translates each of the measured spectra (I_{n-12-i} in the input SDS product from voltage quantities with units of [Volts/(cm^{-1})] to an optical power quantities with units of [either Watts/m^2/(cm^{-1}) or Janskys]. This conversion occurs on a wavenumber-by-wavenumber basis as in Equation 3.44.

Equation 3.44.

$$B_{14-i}(\sigma) = B_{13-i}(\sigma) \times f_i(\sigma)$$

The exact manner by which the conversion curves, $f_i(\sigma)$, will be derived is still TBD but the current baseline is to perform a calibration observation of a source with a known flux. The spectrum derived for each spectrometer detector $B_{13-i}(\sigma)$ will then be used as the conversion curve for this module.

3.5.3. Removal of Optical Crosstalk

Optical crosstalk is here defined as power from the astronomical sky that should be incident on one detector actually falling on another. It is important to note that in the case of SPIRE, neighboring detectors are separated by approximately twice the of the incident beam, therefore even if a source is on-axis for a given detector, a small fraction of the source power will be incident on the neighboring detectors due to telescope diffraction. Non-neighbouring detectors are sufficiently far apart that they should not pick up any power from an on-axis source.

Optical crosstalk will be characterised by a crosstalk matrix, C_{opt}, analogous to the electrical crosstalk matrix described in Section 3.1.2. Let I_{14} be the input vector of spectral flux densities.

The vector of optical crosstalk-corrected spectral flux densities is then given by $I_{15} = C_{opt} I_{14}$

As an illustration, if there are three detectors, the matrix equation would be

Equation 3.45.

$$\begin{bmatrix} I_{15-1} \\ I_{15-2} \\ I_{15-3} \end{bmatrix} = \begin{bmatrix} O_{11} & O_{21} & O_{31} \\ O_{12} & O_{22} & O_{32} \\ O_{13} & O_{23} & O_{33} \end{bmatrix} \begin{bmatrix} I_{14-1} \\ I_{14-2} \\ I_{14-3} \end{bmatrix}$$

Unlike the case of electrical crosstalk (Section 3.1.2), the diagonal elements are not necessarily equal to unity since optical crosstalk involves loss of power from the primary detector.

The optical crosstalk matrix may be implemented as a calibration file. The method by which the components of the optical crosstalk matrix, C_{opt}, is TBD.

Note

In the absence of optical crosstalk, or if the crosstalk correction is to be omitted, then the non-diagonal coefficients of C_{opt} are set to zero and the diagonal coefficients are set to unity.

3.5.4. Spectral Averaging

This module also computes, on a wavenumber-by-wavenumber basis for each spectrometer detector, the average of the spectral intensities across all scans (see Equation 3.46).

Equation 3.46.

$$\overline{I_{16-i}(\sigma_k)} = \frac{1}{N_{scans}} \sum_{n=i}^{N_{scans}} I_{n-16-i}(\sigma_k)$$

This module also computes, on a wavenumber-by-wavenumber basis for each spectrometer detector, the uncertainty in the spectral average. The uncertainty is calculated as the standard deviation of the spectral components as in Equation 3.47.

Equation 3.47.

$$\delta I_{16-i}(\sigma_k) = \sqrt{\frac{1}{N_{scans}-1} \sum_{n=1}^{N_{scans}} \left(I_{n-16-i}(\sigma_k) - \overline{I_{n-16-i}(\sigma_k)}\right)^2}$$

Appendix A. Appendix

A.1. First Level Deglitching Description

1. **Glitch Identification.** Glitch signatures are detected by performing a local regularity analysis (Holderian analysis) over the wavelet transform modulus maxima lines (WTMML) of the signal.

   Let H be the Holder exponent, s the scale of decomposition, $X_i(s)$ the time (or OPD) domain coordinate of the maxima line for the scale s, then when the scale s goes to zero the corresponding wavelet coefficient, $W(X_i(s),s)$, is given by:

   Equation A.1.

   $$W(X_i(s), s) <= Cs^H$$

   where C is a real constant.

   The scale of decomposition, s, may be expressed over a logarithmic scale as:

   Equation A.2.

   $$s = 2^o \, 2^{v/nV}$$

   where positive integers o, nV, and v (with v < nV) are respectively called octave, number of voices, and voice of the decomposition [1], respectively.

   On each maxima line, the regularity degree of the signal is estimated by computing the slope of the linear regression over the set of points $(\log_2(|W|), \log_2(s))$ over the range of scales [scaleMin, scaleMax]. If the relation is linear, i.e. if the square of its correlation coefficient C is greater than the threshold coefficient *thresholdCorr* then the Holder exponent H can be estimated by the measure of the slope of the relation. Glitches are detected as they are similar to dirac-like signatures and show a Holder exponent (i.e. regularity degree) close to -1, ie in a range [thresholdHolder, hMin] centered over -1.

   Noise can generate false detections (it can be shown that the Holder exponent of a gaussian noise has a value (in mean) of 0.5). In order to minimize the likelihood of these false positives, contraints are applied to the wavelet coefficients. By considering a gaussian noise of standard deviation σ, it can be shown that at the lowest scale of decomposition, the following threshold :

   Equation A.3.

   $$|W| <= \sigma \, \sqrt{(2 \ln N)}$$

   where N is the size of the signal.

   The noise standard deviation σ on the signal can be estimated using the Donoho estimator; at the lowest scale, $\sigma = 0.6745 \times \text{med } |W|$

   For each maxima line, if the value of the wavelet coefficient for the first scale value is greater than the previous threshold an estimate is made of the regularity degree.

   Glitch Removal. Each glitch flagged by the preceding step is characterized by a Holder exponent H and by a maxima line X giving for each scale s the location of the maximum of the modulus of the wavelet coefficient X(s). For a glitch signature (the Holder exponent H ~ -1), it can be shown that the wavelet coefficients W_g are given by:

---

[1] C.Ordenovic, C. Surace, B. Torresani, A. Llebaria, "Glitches detection and signal reconstruction using Holder and wavelet analysis.", ADAIV preprint, 5 March 2007.

Equation A.4.

$W_g = \psi((b-X(s)) / s)$

ψ being the wavelet function.

The glitch coefficients, W_g, are then subtracted from the wavelet coefficients, W, and the signal is locally reconstructed by performing a wavelet transform over the corrected wavelet coefficients.

The parameters that follow are optional and have been optimzed for the SPIRE spectrometer detectors. SPIRE PFM1 data that, by visual inspection, contained 29 glitches was used as a basis for this optimization.

- **scaleMin, scaleMax**: The scale range used for the linear regression. Optimal values are scaleMin = 2 and scaleMax = 8.

- **thresholdHolder and H$_{min}$**: The Holder exponent range used to select a glitch. Optimal values are thresholdHolder = -0.6, H$_{min}$ = -1.3.

- **thresholdCorr** : The square threshold correlation that defines linear behaviour. The optimal value is thresholdCorr = 0.985.

- **voices** : The number of voices used for the scale decomposition. he optimal value is voices = 5.

A.2. Radiation Incident on the SPIRE Spectrometer Detectors

The radiation path through the SPIRE spectrometer is illustrated for one case in Figure A.1.
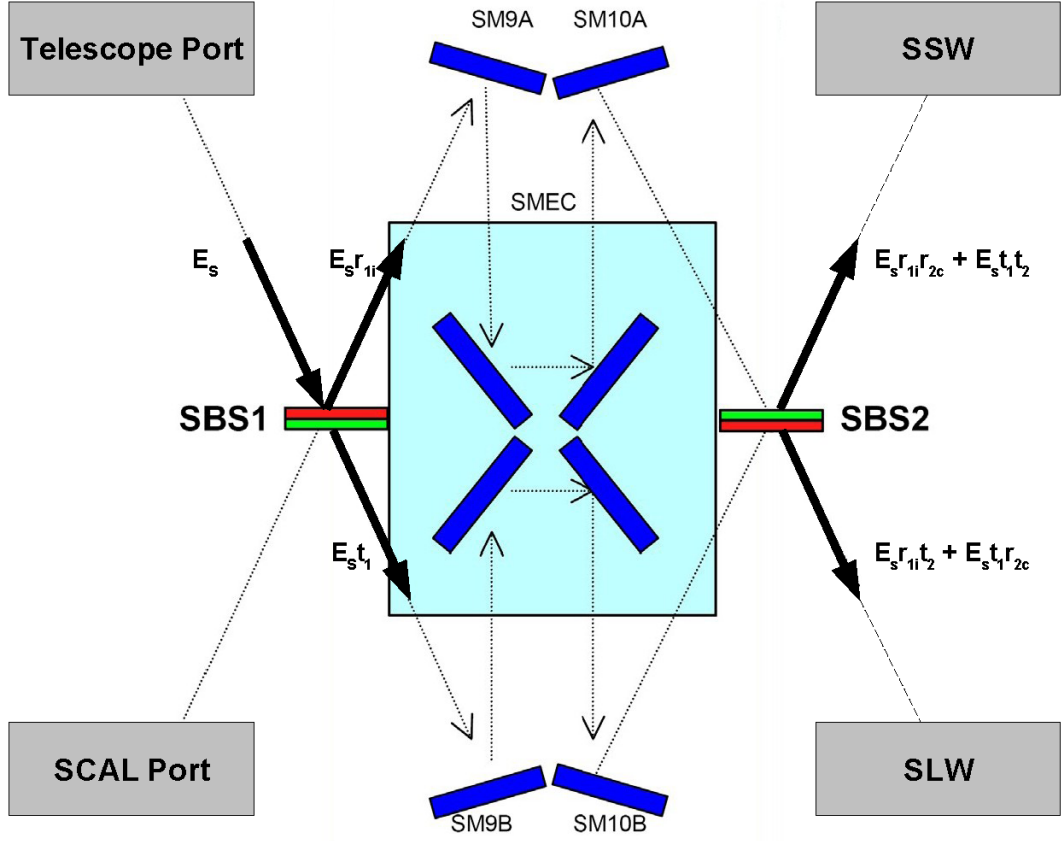
Figure A.1. Radiation from an astronomical source through the SPIRE spectrometer

As shown in Figure A.1, the first beamsplitter (SBS1) divides the incoming electric field (E_S) into two components ($E_S r_{1c}$ and $E_S t_1$). These two components pass through the interferometer and then are split further at the second beamsplitter (SBS2). The upper beam from Figure A.1 then passes to the SSW detectors while the lower beam passes to the SLW detectors. The electric fields incident on the SSW and SLW detectors are given by the following equations:

Equation A.5.

$$E_{S-SSW}(x,\sigma) = E_{S_0}(\sigma)\left[r_{1_i}r_{2_c}\,\mathrm{e}^{-i2\pi(\sigma x_1 - \nu t)} + t_1 t_2\,\mathrm{e}^{-i2\pi(\sigma x_2 - \nu t)}\right]$$

Equation A.6.

$$E_{S-SLW}(x,\sigma) = E_{S_0}(\sigma)\left[r_{1_i}t_2\,\mathrm{e}^{-i2\pi(\sigma x_1 - \nu t)} + t_1 r_{2_i}\,\mathrm{e}^{-i2\pi(\sigma x_2 - \nu t)}\right]$$

At the detectors, the intensity recorded is the time-average of the square of the incident electric field. Using the SSW detectors for illustration, the measured intensity for radiation from an astronomical source at the detectors is given by the following:

Equation A.7.

$$I_S(x,\sigma)=\frac{c\,\epsilon_0}{2}E_S^*(x,\sigma)E_S(x,\sigma)$$

where:

Equation A.8.

$$E_S^*(x,\sigma)E_S(x,\sigma)=E_{S_0}^*(\sigma)\left[r_{1_i}r_{2_c}\mathrm{e}^{i2\pi(\sigma x_1)}+t_1t_2\mathrm{e}^{i2\pi(\sigma x_2)}\right]\times E_{S_0}(\sigma)\left[r_{1_i}r_{2_c}\mathrm{e}^{-i2\pi(\sigma x_1)}+t_1t_2\mathrm{e}^{-i2\pi(\sigma x_2)}\right]$$

Equation A.9.

$$E_S^*(x,\sigma)E_S(x,\sigma)=E_{S_0}^2(\sigma)\left[\left(r_{1_i}r_{2_c}\right)^2+\left(t_1t_2\right)^2+2r_{1_i}r_{2_c}t_1t_2\cos 2\pi\sigma(x_1-x_2)\right]$$

Combining the above results in the following equations for the measured intensity at the SSW and SLW detectors for radiation from an astronomical source:

Equation A.10.

$$\begin{aligned}
I_{SSW}(x)&=\int_0^\infty I_{SSW}(x,\sigma)\,d\sigma\\
&=\int_0^\infty E_0^2(\sigma)\left[\left(r_{1_i}r_{2_c}\right)^2+\left(t_1t_2\right)^2+2r_{1_i}r_{2_c}t_1t_2\cos(2\pi\sigma x)\right]d\sigma\\
&=I_{SSW}(0)\left[\left(r_{1_i}r_{2_c}\right)^2+\left(t_1t_2\right)^2\right]+2\int_0^\infty\left[r_{1_i}r_{2_c}t_1t_2\right]B(\sigma)\cos(2\pi\sigma x)\,d\sigma\\
&=I_{SSW-Offset}+I_{SSW-Modulated}(x)
\end{aligned}$$

Equation A.11.

$$\begin{aligned}
I_{SLW}(x)&=\int_0^\infty I_{SLW}(x,\sigma)\,d\sigma\\
&=\int_0^\infty E_0^2(\sigma)\left[\left(r_{1_i}t_2\right)^2+\left(t_1r_{2_i}\right)^2-2r_{1_i}r_{2_i}t_1t_2\cos(2\pi\sigma x)\right]d\sigma\\
&=\left[\left(r_{1_i}t_2\right)^2+\left(t_1r_{2_i}\right)^2\right]I_{SSW}(0)-2\int_0^\infty\left[r_{1_i}r_{2_i}t_1t_2\right]B(\sigma)\cos(2\pi\sigma x)\,d\sigma\\
&=I_{SLW-Offset}+I_{SLW-Modulated}(x)
\end{aligned}$$

In addition to the astronomical source, radiation from the Herschel telescope and the three components of SCAL (SCAL2, SCAL4, and SCAL) is incident on the SPIRE spectrometer detectors. For the telescope radiation, its path through the SPIRE spectrometer is the same as that for the astronomical source. The path for the SCAL emitters is slightly different (see Figure A.1). The equations for the radiation incident on the SSW and SLW detectors are given by the following:

Equation A.12.

$$I_{SSW}(x) = \int_0^\infty I_{SSW}(x,\sigma)\, d\sigma$$

$$= \int_0^\infty E_0^2(\sigma)\left[\left(r_{1_c}t_2\right)^2 + \left(t_1 r_{2_c}\right)^2 - 2 r_{1_c} r_{2_c} t_1 t_2 \cos(2\pi\sigma x)\right] d\sigma$$

$$= \left[\left(r_{1_c}t_2\right)^2 + \left(t_1 r_{2_c}\right)^2\right] I_{SSW}(0) - 2\int_0^\infty \left[r_{1_c} r_{2_c} t_1 t_2\right] B(\sigma) \cos(2\pi\sigma x)\, d\sigma$$

$$= I_{SSW-Offset} + I_{SSW-Modulated}(x)$$

Equation A.13.

$$I_{SLW}(x) = \int_0^\infty I_{SLW}(x,\sigma)\, d\sigma$$

$$= \int_0^\infty E_0^2(\sigma)\left[\left(r_{1_c} r_{2_i}\right)^2 + \left(t_1 t_2\right)^2 + 2 r_{1_c} r_{2_i} t_1 t_2 \cos(2\pi\sigma x)\right] d\sigma$$

$$= \left[\left(r_{1_c} r_{2_i}\right)^2 + \left(t_1 t_2\right)^2\right] I_{SSW}(0) + 2\int_0^\infty \left[r_{1_c} r_{2_i} t_1 t_2\right] B(\sigma) \cos(2\pi\sigma x)\, d\sigma$$

$$= I_{SLW-Offset} + I_{SLW-Modulated}(x)$$

Taken together, the overall intesity of the radiation measured by the SPIRE spectrometer detectors is given by the following:

Equation A.14.

$$I_{TOTAL}(x) = I_{Source}(x) + I_{Telescope}(x) + I_{SCAL}(x) + I_{SCAL2}(x) + I_{SCAL4}(x)$$

1. **SSW Detectors.**

   Equation A.15.

   $$I_{SSW}(x) = \left(I_{Source}(0) + I_{Telescope}(0)\right)\left[\left(r_{1_i} r_{2_c}\right)^2 + \left(t_1 t_2\right)^2\right] + \left(I_{SCAL}(0) + I_{SCAL2}(0) + I_{SCAL4}(0)\right)\left[\left(r_{1_c} t_2\right)^2 + \left(t_1 r_{2_c}\right)^2\right]$$

   $$+ 2\int_0^\infty \left[r_{1_i} r_{2_c} t_1 t_2\right] B_{Source}(\sigma) \cos(2\pi\sigma x)\, d\sigma + 2\int_0^\infty \left[r_{1_i} r_{2_c} t_1 t_2\right] B_{Telescope}(\sigma) \cos(2\pi\sigma x)\, d\sigma$$

   $$- 2\int_0^\infty \left[r_{1_c} r_{2_c} t_1 t_2\right] B_{SCAL}(\sigma) \cos(2\pi\sigma x)\, d\sigma - 2\int_0^\infty \left[r_{1_c} r_{2_c} t_1 t_2\right] B_{SCAL2}(\sigma) \cos(2\pi\sigma x)\, d\sigma$$

   $$- 2\int_0^\infty \left[r_{1_c} r_{2_c} t_1 t_2\right] B_{SCAL4}(\sigma) \cos(2\pi\sigma x)\, d\sigma$$

2. **SLW Detectors.**

   Equation A.16.

$$I_{SLW}(x) = \left(I_{Source}(0) + I_{Telescope}(0)\right)\left[\left(r_{1_i} t_2\right)^2 + \left(t_1 r_{2_i}\right)^2\right] + \left(I_{SCAL}(0) + I_{SCAL2}(0) + I_{SCAL4}(0)\right)\left[\left(r_{1_c} r_{2_i}\right)^2 + \left(t_1 t_2\right)^2\right]$$

$$-2\int_0^\infty \left[r_{1_i} r_{2_i} t_1 t_2\right] B_{Source}(\sigma)\cos(2\pi\sigma x)\,d\sigma - 2\int_0^\infty \left[r_{1_i} r_{2_i} t_1 t_2\right] B_{Telescope}(\sigma)\cos(2\pi\sigma x)\,d\sigma$$

$$+2\int_0^\infty \left[r_{1_c} r_{2_c} t_1 t_2\right] B_{SCAL}(\sigma)\cos(2\pi\sigma x)\,d\sigma + 2\int_0^\infty \left[r_{1_c} r_{2_i} t_1 t_2\right] B_{SCAL2}(\sigma)\cos(2\pi\sigma x)\,d\sigma$$

$$+2\int_0^\infty \left[r_{1_c} r_{2_i} t_1 t_2\right] B_{SCAL4}(\sigma)\cos(2\pi\sigma x)\,d\sigma$$

A.3. Double-sided and Single-sided Interferograms

The terms double-sided and single-sided as used in this document describe the two types of interferograms that can be measured with a Fourier Transform Spectrometer.

A.3.1. Double-sided Interferograms

Double-sided interferograms are defined as those interferograms or that portion of measured interferogram where the sample *positions* are symmetric about the position of zero path difference (ZPD). That is, a double-sided interferogram is one that contains an equal number of samples before and after the ZPD sample [2]. An envelope of a double-sided interferogram is shown in Figure A.2.
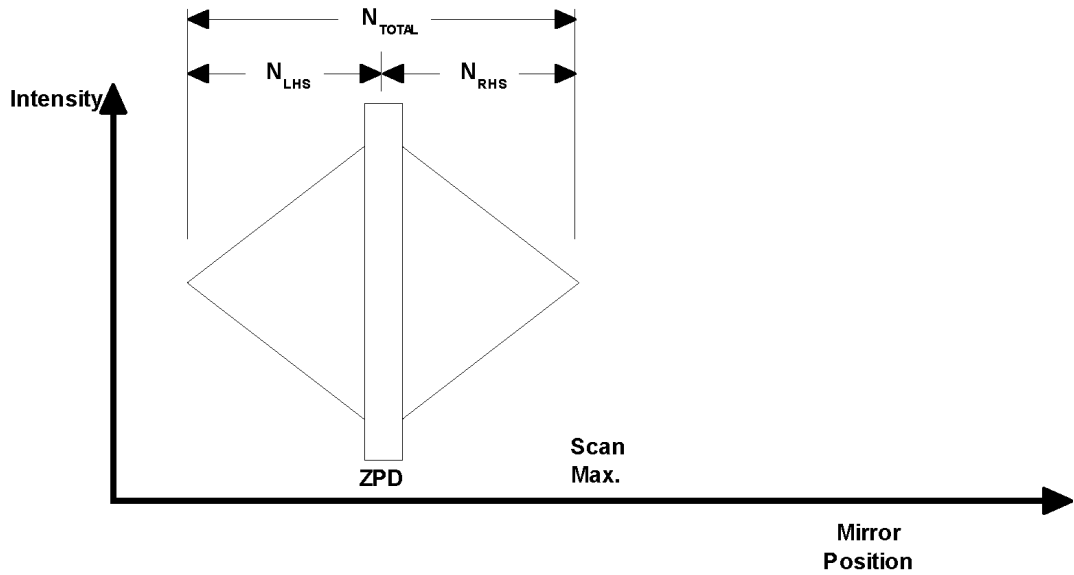

Figure A.2. Envelope of a double-sided interferogram

A.3.2. Single-sided Interferograms

Single-sided interferograms are defined as those interferograms that contain more samples on one side of ZPD than the other. An envelope of a single-sided interferogram is shown in Figure A.3.

---

[2] Some implementations of the Fourier Transform may require an even number of points (N_{TOTAL} even). In this case, the RHS of the double-sided interferogram will contains an extra point to render the total number of points even.
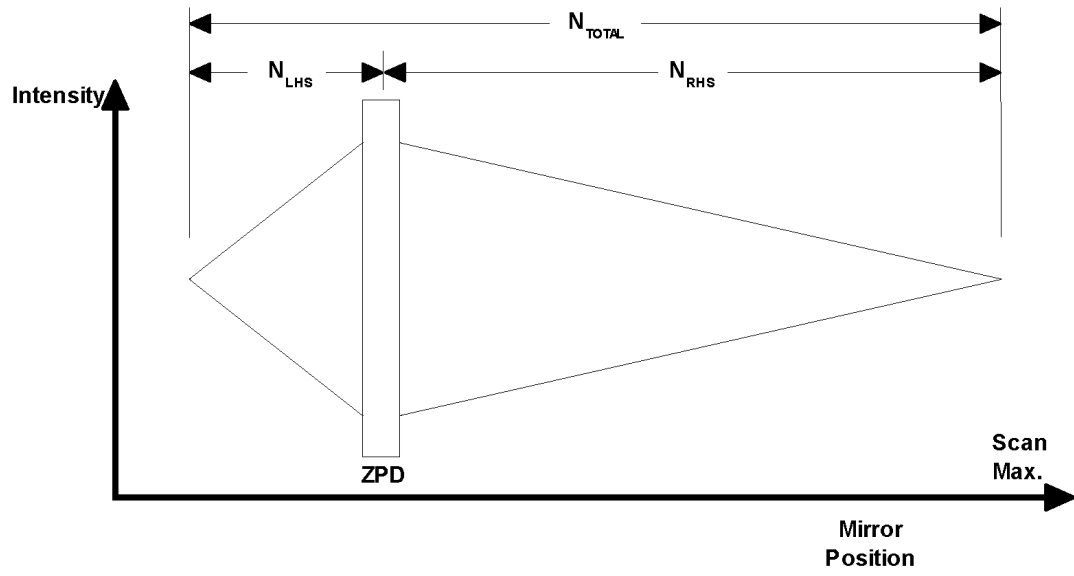
Figure A.3. Envelope of a single-sided interferogram